Ab initio ^{27}Al NMR chemical shifts and quadrupolar parameters for Al_2O_3 phases and their precursors

Ary R. Ferreira,[1] Emine Küçükbenli,[2,3] Alexandre A. Leitão,[1] and Stefano de Gironcoli[2,3]
[1]*Universidade Federal de Juiz de Fora (UFJF), Department of Chemistry, Juiz de Fora, MG, 36036-330, Brazil*
[2]*Scuola Internazionale Superiore di Studi Avanzati (SISSA), Via Bonomea 265, IT-34136 Trieste, Italy*
[3]*CNR-IOM DEMOCRITOS Simulation Center, Via Bonomea 265, IT-34136 Trieste, Italy*
(Received 15 September 2011; published 6 December 2011)

The gauge-including projector augmented wave (GIPAW) method, within the density functional theory (DFT) generalized gradient approximation (GGA) framework, is applied to compute solid state NMR parameters for ^{27}Al in the α, θ, and κ aluminium oxide phases and their gibbsite and boehmite precursors. The results for well established crystalline phases compare very well with available experimental data and provide confidence in the accuracy of the method. For γ-alumina, four structural models proposed in the literature are discussed in terms of their ability to reproduce the experimental spectra also reported in the literature. Among the considered models, the $Fd\bar{3}m$ structure proposed by Paglia *et al.* [Phys. Rev. B **71**, 224115 (2005)] shows the best agreement. We attempt to link the theoretical NMR parameters to the local geometry. Chemical shifts depend on coordination number but no further correlation is found with geometrical parameters. Instead, our calculations reveal that, within a given coordination number, a linear correlation exists between chemical shifts and Born effective charges.

DOI: 10.1103/PhysRevB.84.235119 PACS number(s): 31.15.A−, 76.60.−k, 61.05.Qr, 82.56.Ub

I. INTRODUCTION

Aluminium oxide (Al_2O_3), also known as alumina, is one of the most important oxides because of its many industrial applications.[1] Corundum (α-Al_2O_3), the most stable and common crystalline form of alumina, is the final product of the calcination of hydroxides or oxyhydroxides of aluminium at temperatures above 1273 K, which can vary according to the precursor. The transformation from aluminium hydrates to the final oxide is not direct and a variety of relatively stable intermediate phases can be detected for each combination of starting compound and thermal treatment.

The most commonly used precursors in the synthesis of the various alumina phases are gibbsite [γ-$Al(OH)_3$], bayerite [α-$Al(OH)_3$], and boehmite [γ-AlO(OH)]. The transformation of gibbsite to corundum can proceed through a sequence of hexagonal close packed aluminas (χ and κ) or an alternative sequence in which boehmite is initially formed and the α phase is achieved via the cubic spinel transition phases (γ, δ, and θ).[2] Bayerite can also follow this same sequence through boehmite to form corundum[3] or an alternative path transforming to η and θ phases.[4]

Among the transition aluminas, the γ phase is highly valued for industrial applications due to its textural properties (surface area, pore volume, and pore size), which makes it an important material in many industrial processes acting as an adsorbent, a catalyst and/or catalyst support. In petroleum and petrochemical industries, γ-alumina is used as catalyst support for transition-metal sulfides Co(Ni)MoS in hydrotreatment catalysts and metallic alloys in reforming catalysts.[6,7] Due to its low crystallinity and the consequent difficulty in characterization, the debate on the structure of γ-alumina remains open and a series of theoretical and experimental works concerning this subject have been published along the decades.[8–17]

Since the transition between the distinct intermediate phases is a gradual process, the precise temperature at which each phase is obtained with a high degree of purity can not be determined by x-ray diffraction (XRD) experiments only. Solid-state nuclear magnetic resonance (SS-NMR) is an important technique for material characterization. Long-range order is not a prerequisite to distinguish different phases and the knowledge of ^{27}Al NMR data can allow the detection of the onset of phase changes during alumina calcination,[18] permitting a discussion of the transition mechanisms.[19] A detailed interpretation of the results remains, however, a challenge.

The advent of theoretical techniques such as the gauge-including projector augmented wave (GIPAW) method[20,21] enables the *ab initio* calculation of isotropic chemical shielding, σ_{iso}, quadrupolar coupling constant, C_Q, and asymmetry parameter, η_Q, in solids. First-principles simulations of NMR spectra of structural models for transition aluminas are now possible[22,23] and can be compared with available experimental data.

In this paper, we apply the GIPAW method to compute solid-state magic angle spinning (MAS) NMR parameters for a number of well characterized aluminium oxide phases and for their boehmite and gibbsite precursors. The results are compared with available experimental data to validate the method. In order to contribute to a better characterization of γ-alumina, a number of structural models proposed in the literature are examined and their simulated spectra compared to experimental ones, thus revealing their adequacy.

We then examine possible correlations of the predicted chemical shifts with local atomic geometry or local electronic structure, described through Bader analysis[24] and Born dynamical effective charges,[25] finding significant correlations.

The rest of the paper is organized as follows: in Sec. II, we describe the theoretical methodology and the structural models used. In Sec. III, we present our calculated NMR results, compare them with experiments and discuss the resulting correlations. Section IV, contains our conclusions.

II. DETAILS OF CALCULATIONS

A. Electronic structure

All *ab initio* calculations in this study were performed using the codes available within the QUANTUM ESPRESSO distribution,[26] which implements the DFT[27] framework using a plane-wave basis set to expand the one-electron wave functions of Kohn-Sham equations.[28] The effect of exchange-correlation (XC) potential was explored by comparing the results of different descriptions for this term: Perdew-Burke-Ernzerhof (PBE) generalized gradient approximation[29] and its revision (revPBE) by Zhang and Yang.[30] Furthermore, we also considered a van der Waals-aware density functional (vdW-DF)[31,32] recently implemented in QUANTUM ESPRESSO. Interaction of valence electrons with nuclei and core electrons were treated by the projector augmented-wave (PAW)[33] method.

The plane-wave kinetic energy cutoff and k-points sampling were adjusted to yield less than 1 mRy/atom convergence in total energy for all models. A kinetic energy cutoff of 45 Ry and expansion of augmentation charges up to 220 Ry were sufficient to ensure this criterion. Integration in the Brillouin zone were determined by the Monkhorst-Pack[34] procedure.[35] Both atomic positions and cell vectors were fully optimized. NMR chemical shieldings were converged within less than 1 ppm.

The Born effective charge tensor $Z^*_{\kappa,\alpha\beta}$ is defined[25] by the macroscopic polarization induced in direction β and under conditions of zero macroscopic electric field, by a zone-center phonon displacing atomic sublattice κ in direction α. Effective charges were calculated within density functional perturbation theory (DFPT)[36,37] and the values presented in the following sections correspond to their isotropic component obtained by $Z^*_\kappa = \mathrm{Tr}[Z^*_{\kappa,\alpha\beta}/3]$.

B. NMR chemical shifts and quadrupolar parameters

First-principles GIPAW calculations[20,21] yield the absolute chemical shielding tensors for each nucleus, $\vec{\sigma}(r)$. Isotropic chemical shieldings, $\sigma_{\mathrm{iso}} = \mathrm{Tr}[\vec{\sigma}/3]$, are compared to the experimental isotropic chemical shifts by using the standard expression: $\delta_{\mathrm{iso}} = \sigma_{\mathrm{ref}} - \sigma_{\mathrm{iso}}$. In this work, we choose corundum as reference such that ^{27}Al shift of the α phase is aligned to the experimental one at 0 ppm.

The resulting *ab initio* NMR spectra were obtained by using the QUADFIT program[38] with the theoretically calculated chemical shifts and quadrupolar interaction parameters, using the experimental magnetic field intensity, and normalizing each spectral component to reflect the relative number of aluminium types. A Lorentzian broadening was added to each spectral feature to obtain the best comparison with the experimental line shape.

C. Structural models

Among the oxide phases with well characterized structures, we studied the final product α and the transitional aluminas θ and κ. The structural model for α-alumina, used as a reference for all simulated NMR spectra in this work, was published by Ishizawa *et al.*[39] in an XRD study. The structure was reported as a corundum type, with a hexagonal crystal system and $R\bar{3}c$ space group. The crystallographic cell contains six Al_2O_3 units in which all aluminium sites are coordinated by six oxygens.

The θ phase is present along the $\gamma \rightarrow \alpha$ transition in different dehydration paths and its structure has been characterized by Zhou and Snyder,[9] with a monoclinic crystal system and $C2/m$ space group. In that work, the structure was refined from Rietveld analysis resulting in a crystallographic cell with four Al_2O_3 units, in which half of the aluminium atoms are octahedrally (Al_{oct}) and half are tetraedrally (Al_{tet}) coordinated.

The κ phase is one of the intermediate products of the dehydration path from gibbsite to corundum. Ollivier *et al.*[40] describes the κ phase with an orthorhombic system and $Pna2_1$ space group. The cell contains six Al_2O_3 units and 25% of the Al^{3+} sites are tetrahedral, 50% octahedral, and 25% in a very distorted octahedral.

We have also studied the NMR spectra of precursor phases gibbsite and boehmite. For gibbsite, we started from the structure resolved by Saalfeld and Wedde in a single-crystal XRD study.[41] The structure is monoclinic with $P2_1/n$ space group where the Al^{3+} cations are octahedrally coordinated by 6 OH^- groups forming double layers and occupy two thirds of the octahedral holes in alternate layers.[42] The interlayer cohesion is granted by hydrogen bonds between these OH^- groups.

In the also layered boehmite structure, described by Christensen *et al.*,[43] each Al^{3+} cation is octahedrally coordinated by 2 OH^- groups and 4 intralayer O^{2-} anions in an orthorhombic system with $Cmcm$ space group. As in the gibbsite structure, the boehmite double layers interact with each other via hydrogen bonds, which are exclusively interlayer. In this phase, hydrogen bonds are organized in chains along [001] direction and different bond networks are possible depending on the relative orientation of neighboring chains. In our calculations, we considered all possible combinations compatible with a 2×2 supercell. The structure with the lowest energy was found to be the one where nearest-neighbor chains are antiparallel. However, energy differences among various combinations are found to be less than 1 mRy/cell, which is consistent with the experimentally observed disorder in this phase.[44]

As one of the aims of this work is to contribute to the characterization of γ-alumina phase, four different γ-alumina structural models from published theoretical works have been studied.

The first γ-phase model, γ-$Al_2O_3(A)$, considered here was proposed by Gutierrez *et al.*[45,46] This model, also called *defect spinel* or *spinel-like* structure, consists of a cell with eight Al_2O_3 units, in which 37.5% of the cations are Al_{tet} and 62.5% are Al_{oct}. Among the 24 O atoms, 12 are fourfold coordinated ($O_{fourfold}$) and 12 are three-fold coordinated ($O_{threefold}$) to aluminium atoms.[47] It is important to note that in this model only spinel sites are occupied by the Al^{3+} cations.

The next γ-phase model, γ-$Al_2O_3(B)$, used in this work was published by Digne *et al.*[7] and proposed by Krokidis *et al.*[14] The model has eight Al_2O_3 units in the cell, 25% of all aluminium atoms are Al_{tet} sites, in a sublattice of O^{2-} anions. The crystal system is monoclinic, but very close to an orthorhombic one with the $P2_1/m$ space group. In this model, cations occupy also nonspinel sites.

Two other γ-phase models were published by Paglia *et al.*[48,49] The unit cells of these models contain a large number of atoms, 32 Al_2O_3 units, and were generated from an extensive search on all structural possibilities of the γ-Al_2O_3 structures using $Fd\bar{3}m$ and $I4_1/amd$ space groups. In the $Fd\bar{3}m$ model, γ-$Al_2O_3(C)$, among the 64 Al^{3+} sites 22 are Al_{tet}, 41 are Al_{oct} and 1 is Al_{pen} (five-coordinated), while in the $I4_1/amd$ model, γ-$Al_2O_3(D)$, there are 21 Al_{tet} and 43 Al_{oct} sites. In these two models, due to the breaking of the local symmetry by the variations in cation occupancies and related distortions in octahedral and tetrahedral sites, the symmetry is actually P_1.[50]

III. RESULTS AND DISCUSSION

A. Structure optimization and approximations on exhange-correlation functional

Geometry optimization was performed for all phases, allowing both the atomic positions and cell vectors to relax keeping the group symmetry fixed. To investigate the effect of approximations on exhange-correlation functionals, each geometry optimization was repeated with PBE, rev-PBE, and the vdW-DF functionals as described in Sec. II A. All XC functionals considered overestimate the experimental volume, PBE by about 1.8% on average, revPBE by 4.2%. The use of van der Waals functional was found to have negligible effect, inducing a tiny further expansion, on all structures except for gibbsite [γ-$Al(OH)_3$] (see Table I) where a slight contraction was observed. The exception in the case of gibbsite can be understood considering its layered and open structure.

Since *ab initio* NMR calculations are very sensitive to structural details, we performed all NMR calculations at optimized positions for each XC functional. In spite of the discrepancy in calculated equilibrium volume, the average difference in σ_{iso}, $|C_Q|$, and η_Q between PBE and rev-PBE were calculated as 1.15 ppm, 0.14 MHz, and 0.03, respectively. These values were found to have negligible effect on total spectra and, except for gibbsite, only the PBE spectra will be shown. The numerical values for the three XC functionals are reported in Table II.

TABLE I. Volumes of the experimental and optimized cells with PBE, rev-PBE, and vdW-DF functionals for the five phases with well characterized experimental structures considered in this work.

	Volume (Å^3)			
Structure	Experiment	PBE	rev-PBE	vdW-DF
α-Al_2O_3	254.25[a]	261.84	266.30	268.06
θ-Al_2O_3	187.92[b]	192.53	195.54	196.34
κ-Al_2O_3	361.31[c]	369.19	375.21	377.75
γ-AlO(OH)	261.13[d]	262.61	270.24	271.65
γ-$Al(OH)_3$	427.98[e]	431.57	449.51	447.30

[a]Reference 39.
[b]Reference 9.
[c]Reference 40.
[d]Reference 43.
[e]Reference 41.

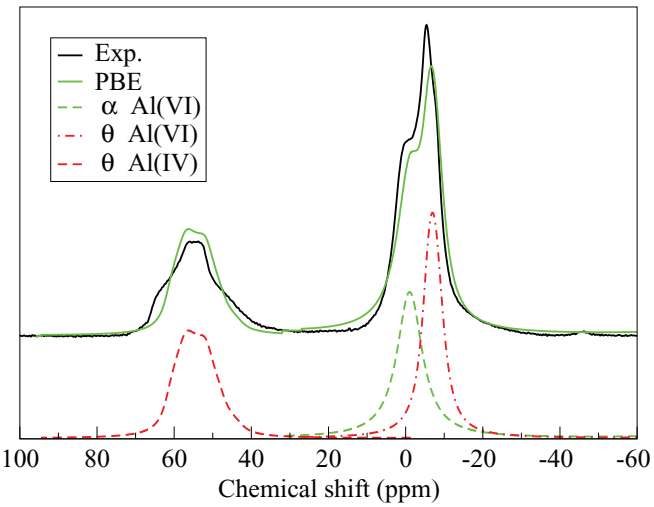

FIG. 1. (Color online) Comparison between our theoretical results and the experimental ^{27}Al MAS NMR spectra from Ref. 19 for a mixture of the α and θ alumina phases (upper curves) obtained at 14.1 T. Decomposition of the theoretical spectrum in its individual components is also given (lower curves).

B. NMR parameters and spectra for well characterized structures

In this section, we present a detailed comparison of our *ab initio* calculated chemical shifts and quadrupolar interaction parameters for all the well characterized structural phases mentioned in Sec. II C with experimental data, as well as with very recent theoretical results from the literature. All relevant data are shown in Table II.

1. α and θ phases

Corundum, α-Al_2O_3, shows a single well defined NMR peak that we take as reference when comparing spectra for other structures. For the θ phase, we compare our results with the ones reported in Ref. 19, where a mixture of α and θ phases were examined, and the NMR parameters (see Table II) for these two coexisting phases were extracted from the experimental spectrum by line-shape fitting.

The overall good agreement between experimental and theoretical spectra can be seen in Fig. 1, upper curves. The decomposition in individual contributions is also given. The main difference between experiment and theory is in the asymmetry parameter η_Q for the Al_{tet} site. For this peak, it should be noted that a recent theoretical work[23] has also reported a value similar to ours.

2. κ phase

The crystal structure of κ-alumina has been reported in a work by Ollivier *et al.*[40] in which ^{27}Al MAS NMR and multiple quantum magic angle spinning (3Q MQ MAS) ^{27}Al NMR experiments were also performed and interpreted on the basis of the local structure. Three distinct resonance signals were identified in the spectrum obtained with magnetic field intensity of 7.0 T, two of them from Al_{oct} sites. At a higher magnetic field of 11.7 T, further resolution revealed an additional peak for this site at high shielding, resulting in the interpretation of the complex line shape for Al_{oct} peak

TABLE II. Comparison between chemical shifts and quadrupolar coupling parameters calculated in this work and experimental and theoretical data from the literature.

	δ_{iso} (ppm)			C_Q (MHz)			η_Q		
Structure	previous		this work	previous		this work	previous		this work
Al site	Exp.	Th.	PBE/rev-PBE/vdW-DF	Exp.	Th.	PBE/rev-PBE/vdW-DF	Exp.	Th.	PBE/rev-PBE/vdW-DF
α-Al_2O_3									
Al_{oct}	0.0 (1)[a]	0.0[b]	0.0	2.38[a]	2.33[b]	2.05/1.98/2.10	0.00[a]	0[b]	0.04/0.04/0.03
θ-Al_2O_3									
Al_{oct}	−3.0 (1.0)[a]	−5.9[b]	−4.9/−4.8/−5.0	3.50 (0.30)[a]	3.44[b]	2.91/2.81/2.71	0.00 (0.10)[a]	0.18[b]	0.26/0.36/0.29
Al_{tet}	66.5 (1.0)[a]	62.3[b]	62.6/60.2/61.1	6.40 (0.10)[a]	6.34[b]	5.63/5.53/5.37	0.65 (0.02)[a]	0.42[b]	0.43/0.37/0.42
κ-Al_2O_3									
$Al_{oct}(1)$[f]	0.0[c]	0.3[b]	2.0/2.3/2.0	0.50[c]	−9.98[b]	−9.53/−9.45/−9.41	...	0.33[b]	0.29/0.29/0.28
$Al_{V+I}(2)$[f]	...	4.4[b]	7.1/6.7/6.8	>1.5[c]	4.51[b]	4.43/4.33/4.27	...	0.77[b]	0.76/0.77/0.68
$Al_{tet}(3)$[f]	68.5[c]	60.7[b]	62.6/60.2/61.2	0.76[c]	−5.53[b]	−4.83/−4.67/−4.49	0.3[c]	0.33[b]	0.33/0.31/0.32
$Al_{oct}(4)$[f]	5.0[c]	1.4[b]	3.8/3.6/3.5	0.85[c]	5.20[b]	4.99/−4.96/5.06	...	0.94[b]	0.99/1.00/1.00
γ-$Al(OH)_3$ Gibbsite									
$Al_{oct}(1)$	−5.6[d,g]	2.2[e]	2.2/2.3/2.1[h]	4.70 ± 0.20[d]	5.10[e]	−5.30/−4.74/−4.43	1.00 ± 0.05[d]	0.35[e]	0.32/0.35/0.35
$Al_{oct}(2)$	0.0[d,g]	0.0[e]	0.0[h]	2.20 ± 0.20[d]	2.80[e]	2.33/2.06/1.81	0.75 ± 0.05[d]	0.66[e]	0.81/0.71/0.66
γ-AlO(OH) Boehmite									
Al_{oct}	−1.0[d,g]	...	−0.9/−0.5/−0.2[h]	1.8–2.8[d]	...	2.16/2.08/2.27	0.5–1.0[d]	...	0.45/0.46/0.67

[a]Reference 19.
[b]Reference 23.
[c]Reference 40.
[d]Reference 44.
[e]Reference 51.
[f]Aluminium sites are labeled according to Ref. 40 and the sites symmetry, see Table III.
[g]The experimental $\delta_{iso}[Al_{oct}(2)] = 11.5 \pm 0.2$ ppm from gibbsite is taken as reference.
[h]The calculated $\sigma_{iso}[Al_{oct}(2)] = 562.72$ ppm from gibbsite is taken as reference.

region as the overlap of three distinct peaks: two with high, one with low quadrupolar coupling. The high-coupling component was assigned to the strongly distorted Al_{oct} site, Al(2) in the published crystallographic description, and was labeled as Al_{V+I} to stress the presence of a strongly elongated Al-O bond.

In order to discuss the local distortion of the aluminium sites, we calculated the average absolute deviation in distances

$$D_{dist} = \sum_{i=1}^{n} \frac{|d_i - \overline{d}|}{n}, \quad (1)$$

where $n = 4$ or 6 for Al_{tet} and Al_{oct} sites, respectively. The angular deviation of the O-Al-O angles from their ideal values in octahedra and tetrahedra are calculated as

$$D_{ang} = \sum_{i=1}^{k} \frac{|\beta_i - \beta_{ref}|}{k}, \quad (2)$$

where $k = 6$ and $\beta_{ref} = 109.47^\circ$ for the Al_{tet} sites or $k = 12$ and $\beta_{ref} = 90^\circ$ for the Al_{oct} sites.

As it can be seen in Table III, our calculations confirm the order of increasing distortion in octahedral sites suggested in the experimental analysis and in particular site $Al_{V+I}(2)$ is found to be the most distorted.

The simulated total spectra, reported in Fig. 2, obtained with our calculated δ_{iso}, C_Q, and n_Q, are in very good qualitative agreement with the ^{27}Al MAS NMR experimental spectrum of Ref. 40 at both magnetic field intensities.

However, from the theoretical decomposition of the composite octahedral peak, it can be seen that the high shielding feature around −50 ppm, which was experimentally observed

TABLE III. Optimized Al-O distances for the κ-Al_2O_3 structure. Additionally, for the experimental[40] and the optimized structures, we present the average absolute deviation in the distances, D_{dist}, and in the O-Al-O angles, $D_{ang.}$, according to Eqs. (1) and (2).

	$Al_{oct}(1)$	$Al_{V+I}(2)$	$Al_{tet}(3)$	$Al_{oct}(4)$
Distances (Å)	1.962	1.991	1.797	1.879
	1.961	2.269	1.772	1.959
	1.936	1.848	1.756	1.821
	1.820	1.829	1.784	2.026
	1.917	2.038	...	1.838
	1.968	1.844	...	2.215
D_{dist} (Å)				
Th.	0.039	0.130	0.013	0.111
Exp.	0.058	0.171	0.025	0.105
D_{ang} (degree)				
Th.	5.028	8.392	3.572	7.305
Exp.	5.150	8.590	5.081	6.888

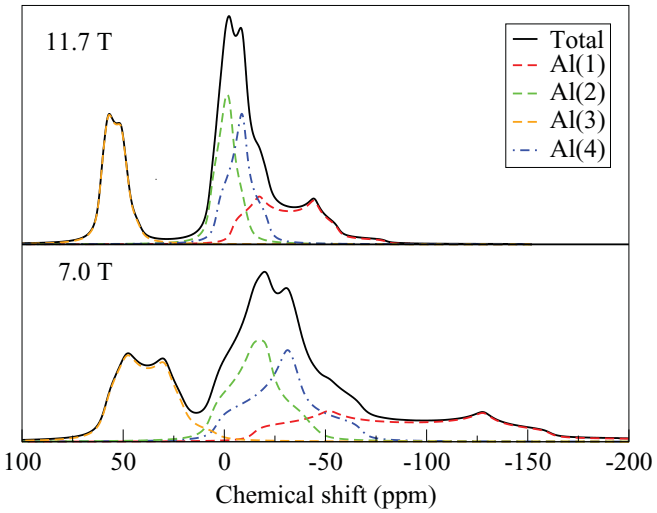

FIG. 2. (Color online) Simulated ^{27}Al MAS NMR spectra for κ-alumina at 11.7 T (upper graph) and 7.0 T (lower graph). Decomposition of the spectra in individual components is also given.

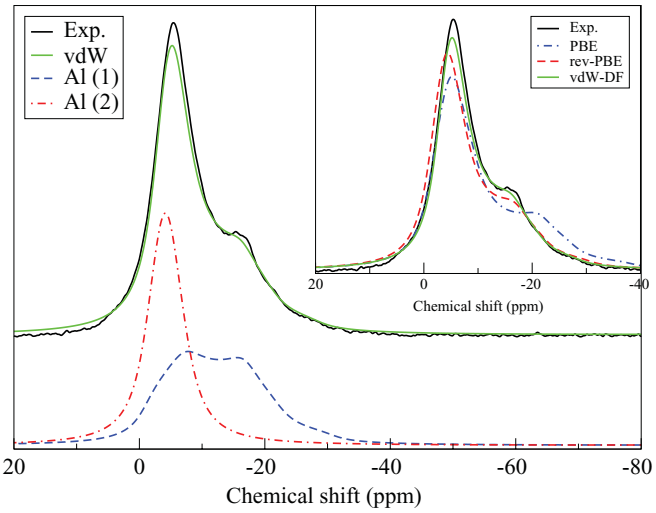

FIG. 3. (Color online) Comparison between the experimental ^{27}Al MAS NMR spectra at 9.4 T from Ref. 18 for gibbsite and the theoretical spectrum obtained with the vdW-DF functional. Decomposition of the spectrum in individual components is also given. The effect of different exchange and correlation functionals on the simulated spectrum is shown in the inset.

at high magnetic field intensity and was assigned to be Al(2) on the basis of the distortion data, is actually part of a bimodal peak with high quadrupolar coupling and low asymmetry parameter, which belongs to Al(1). Morever, the experimental detection of this particular feature only at high field intensity can also be understood considering the *ab initio* spectrum for low field intensity, reported in the lower part of Fig. 2. As can be seen, at low magnetic field intensity, Al(1) peak broadens considerably due to its high quadrupolar coupling constant, making it difficult to observe over the background in the experiment. This demonstrates that, even though experiments can provide accurate structural information, *ab initio* NMR calculations might be essential for an unambiguous peak assignment. Close agreement with previous theoretical calculation[23] further support the present assignment.

3. *Gibbsite and boehmite phases*

The structures and NMR properties of gibbsite and boehmite are experimentally well characterized.[44,51–53] As can be seen in Fig. 3, the gibbsite NMR spectrum simulated with the theoretically determined parameters agrees very satisfactorily with the experimentally obtained spectrum by Hill *et al.*[18] This structure is the only one for which we observed a noticeable dependence of the theoretical spectra on the exchange-correlation functional used, showing improved results when using vdW-DF[31] functional (see inset in Fig. 3). In Table II, we present a quantitative comparison between our calculated NMR parameters and the experimental results reported by Damodaran *et al.*[44] Our results for C_Q and η_Q are in good agreement with both of these experiments and can accurately reproduce the asymmetry of the peak.

In agreement with the previous theoretical work by Vyalikh *et al.*,[51] in Fig. 3, we show that this resonance profile can be decomposed as the superposition of two distinct peaks with different second-order quadrupolar structures, belonging to two distinct Al_{oct} sites in gibbsite.

As described in Ref. 51, the two sites differ in the OH groups surrounding them. This can be seen in Fig. 4 where a single $Al(OH)_3$ layer is drawn showing that among the six OH groups surrounding $Al_{oct}(1)$, two participate in interlayer hydrogen bonds as donors, while the remaining four are oriented in-plane and participate in interlayer hydrogen bonds as acceptors. For $Al_{oct}(2)$, the opposite occurs.

We further characterize the two aluminium sites reporting, in Table IV, the ^{17}O chemical shifts, the Born effective charges and the hydrogen-bond connectivity of the six oxygen types (labeled in Fig. 4) surrounding them. This analysis reveals that the two aluminium sites are mostly surrounded by the same types of oxygens and the distinction is based on just two different oxygen environments (O_c and O_d), each one neighboring only one type of aluminium site.

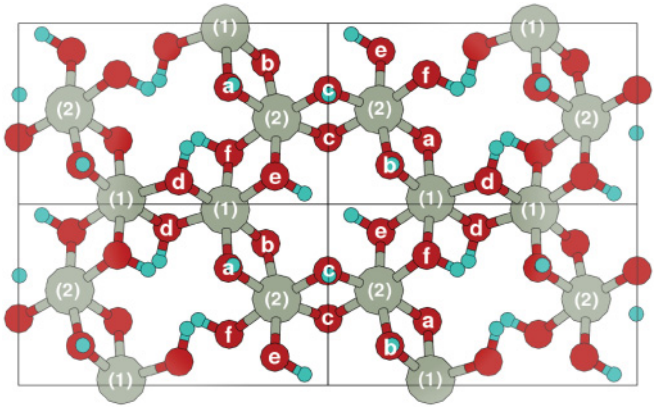

FIG. 4. (Color online) View from direction (001) of a single $Al(OH)_3$ layer in gibbsite showing the arrangement of the different types of hydroxyl groups around the aluminium cations (large gray atoms). Oxygen (small red atoms) are labeled according to their different environments as referred in Table IV.

TABLE IV. Effective charges, chemichal shifts, and hydrogen-bonding properties (ID = interlayer donor, IA = interlayer acceptor) for the different types of oxygen atoms in gibbsite. Labelling according to Fig. 4.

Site	Z^*	σ_{iso}	H bond
O_a	−1.46	238.2	ID
O_b	−1.45	242.4	ID
O_c	−1.43	246.2	ID
O_d	−1.41	229.4	IA
O_e	−1.38	238.4	IA
O_f	−1.36	228.0	IA

The oxyhydroxide polymorph boehmite, γ-AlO(OH), was detected by XRD in the experiment by Hill *et al.*[18] in the temperature range from 200 to 400 °C in a mixture with gibbsite or the transitional χ phase. A direct comparison between a simulated NMR spectrum for this phase with that experiment is therefore not possible. In the experiment by Damodaran *et al.*,[44] the lack of high resolution in the boehmite NMR spectrum is suggested to be due to the disorder in Al positions in the sample used, leading to small variations in the isotropic chemical shift and quadrupolar couplings. Nevertheless, it was possible to extract experimental estimates for C_Q and η_Q, which are in good agreement with our calculated values, as presented in Table II.

C. The γ-Al_2O_3 phase and its structural models

As previously mentioned, γ-alumina structure is not yet well characterized in the literature and a vast discussion about this subject persists. Experimental NMR spectra of γ-alumina have been reported in a number of studies. In the work by O'Dell *et al.*,[19] the samples obtained with calcination temperatures from 600 to 1000 °C are attributed to mixtures of cubic spinel transitional phases, as indicated by the presence of a tetrahedral peak around 60 ppm (taking the α phase as a reference). The fivefold-coordinated peak that has been observed in this phase has been attributed to inherent disorder[19] or surface atom contributions.[54] The MAS NMR study of Pecharromán *et al.*[55] reported a small percentage of AlO_5 sites as well, along with an occupation of 76.3% and 21% for Al_{oct} and Al_{tet} sites, respectively. However, no evidence of a fivefold-coordinated Al peak is present in some other experiments, such as the one of Ref. 56, obtained from a hydrogenated boehmite precursor calcinated at 600 °C for several hours and the one of Ref. 18, in which the sample was obtained from the calcination of gibbsite at 700 °C through the formation of boehmite at 300 °C.

To gain further insight on the structure of this phase, we have calculated the *ab initio* NMR parameters and obtained the simulated spectrum for each one of the four γ-alumina structural models that have been mentioned in Sec. II C. From the comparison of the calculated spectra with the experimental ones obtained for calcination conditions associated to γ-alumina, an evaluation of the adequacy of these structural models will be possible. Since NMR is a sensitive probe of the local structural and chemical environment, comparisons based on NMR parameters will provide complementary constraints with respect to x-ray and neutron diffraction methods used, for instance, in the detailed structural search of Ref. 49.

In Fig. 5, we compare the theoretical spectra with the experimental data by O' Dell *et al.*[19] (left panel, 14.1 T), and by Hill *et al.*[18] (right panel, 9.4 T). We also compared with the 9.4 T spectrum by Pecharromán *et al.*[55] (not shown), which agrees very well with the one by Hill *et al.*

From Fig. 5, it is clear that the simulated MAS NMR spectra for the γ-Al_2O_3(C) structural model proposed by Paglia *et al.*[49] best reproduces all the experimental results considered. The agreement is very satisfactory and even better for the more precise spectrum at the higher magnetic field (left panel of Fig. 5).

It may appear natural that the two models that display lesser agreement with the experimental spectra are the two (models A and B) whose unit cells only contain 8 Al_2O_3 formula units and a reduced number of nonequivalent aluminium environments, while model C contains a large number of Al_2O_3 formula units allowing a distribution of NMR parameters,

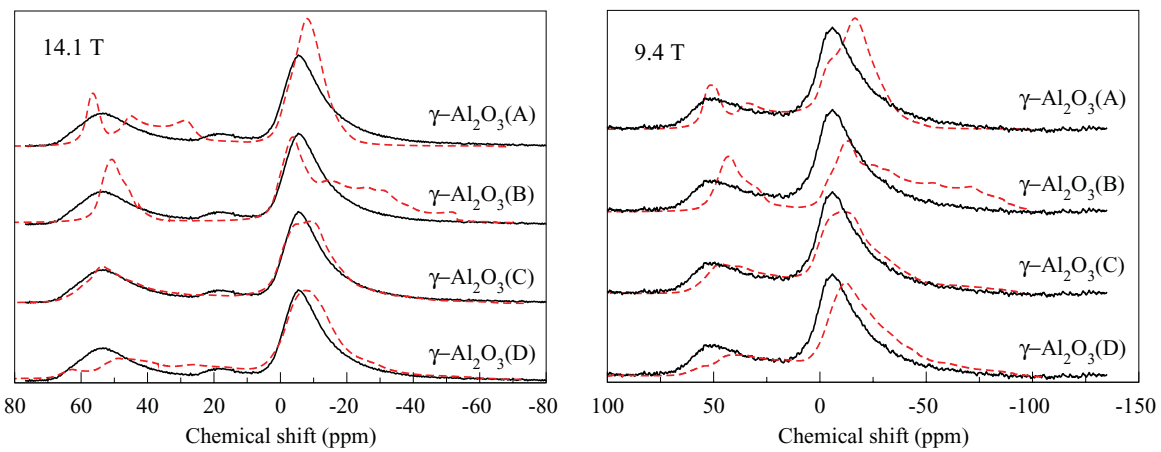

FIG. 5. (Color online) Comparison of the theoretical spectra (dashed red lines) for the four γ-alumina models considered in this study and the experimental ^{27}Al MAS NMR spectra (black solid lines) from Ref. 19 (left panel) and Ref. 18 (right panel). A Lorentzian broadening of 0.5 KHz was added to each component which were properly normalized to reflect relative site abundance.

TABLE V. Average values and corresponding standard deviations for ^{27}Al chemical shifts, absolute quadrupolar coupling, asymmetry parameters, and site occupation, decomposed according to Al coordination number, for the four γ-alumina models considered in this work.

	δ_{iso} (ppm)	$\lvert C_Q \rvert$ (MHz)	η_Q	%
γ-$Al_2O_3(A)$				
AlO_6	-0.6 ± 1.8	4.90 ± 0.47	0.86 ± 0.12	62.5
AlO_4	52.1 ± 3.0	6.36 ± 2.65	0.14 ± 0.08	37.5
γ-$Al_2O_3(B)$				
AlO_6	-0.7 ± 4.9	7.98 ± 3.25	0.41 ± 0.23	75
AlO_4	52.0 ± 0.1	4.51 ± 0.91	0.47 ± 0.35	25
γ-$Al_2O_3(C)$				
AlO_6	-0.8 ± 4.3	5.93 ± 2.45	0.52 ± 0.26	64.0
AlO_5	15.9	7.43	0.34	1.6
AlO_4	59.9 ± 4.7	7.70 ± 3.00	0.64 ± 0.25	34.4
γ-$Al_2O_3(D)$				
AlO_6	-0.1 ± 4.2	6.25 ± 2.38	0.57 ± 0.23	67.2
AlO_4	52.7 ± 6.5	8.27 ± 2.92	0.58 ± 0.27	32.8

which is more suitable for the representation of the broad features observed experimentally. Notice, however, that having a large number of nonequivalent aluminium environments may be considered a necessary, but not a sufficient condition to properly reproduce the experimental NMR spectra. In fact, both Paglia's structural models (C and D) contain 64 Al_2O_3 formula units and reproduce neutron diffraction data[49] equally well but only model C (the one associated to $Fd\bar{3}m$ symmetry) satisfactorily reproduces the spectral region of the tetrahedrally coordinated Al atoms and even for this model the sharpness of the octahedral-Al peak is not completely satisfactory. Table V shows that, on average, model C gives a higher average value for δ_{iso} for the Al_{tet} peak while the other models display rather similar values that underestimate the experiment.

Furthermore, in the γ-Al_2O_3 structural model C, a truly AlO_5 site is evident, and its calculated δ_{iso} of 15.9 ppm is easily separated from the peaks of octahedrally (−9.4 to 9.4 ppm) and tetrahedrally (42.6 to 68.0 ppm) coordinated sites. Although the small occupation of this site in model C cannot reproduce the AlO_5 peak observed by some experiments, the δ_{iso} is in the experimentally measured range, implying that an increase in AlO_5 sites due to defects and/or surface effects would explain the observed feature.

It should be noted that in the study by Pecharromán *et al.*,[55] the complex NMR spectrum in the γ-alumina region was analyzed as superposition of a small number of peaks parameters. for which the quadrupolar interaction parameters were estimated for tetrahedral ($C_Q = 4.7$–4.9 MHz) and octahedral ($C_Q = 3.6$–3.9 MHz) sites. These estimated values do not agree with the ones obtained for model C. Since model C shows very good agreement for the total spectrum, this implies that extracting NMR parameters from a complex spectrum, in absence of further experimental or theoretical characterization, is likely an unreliable procedure as it can

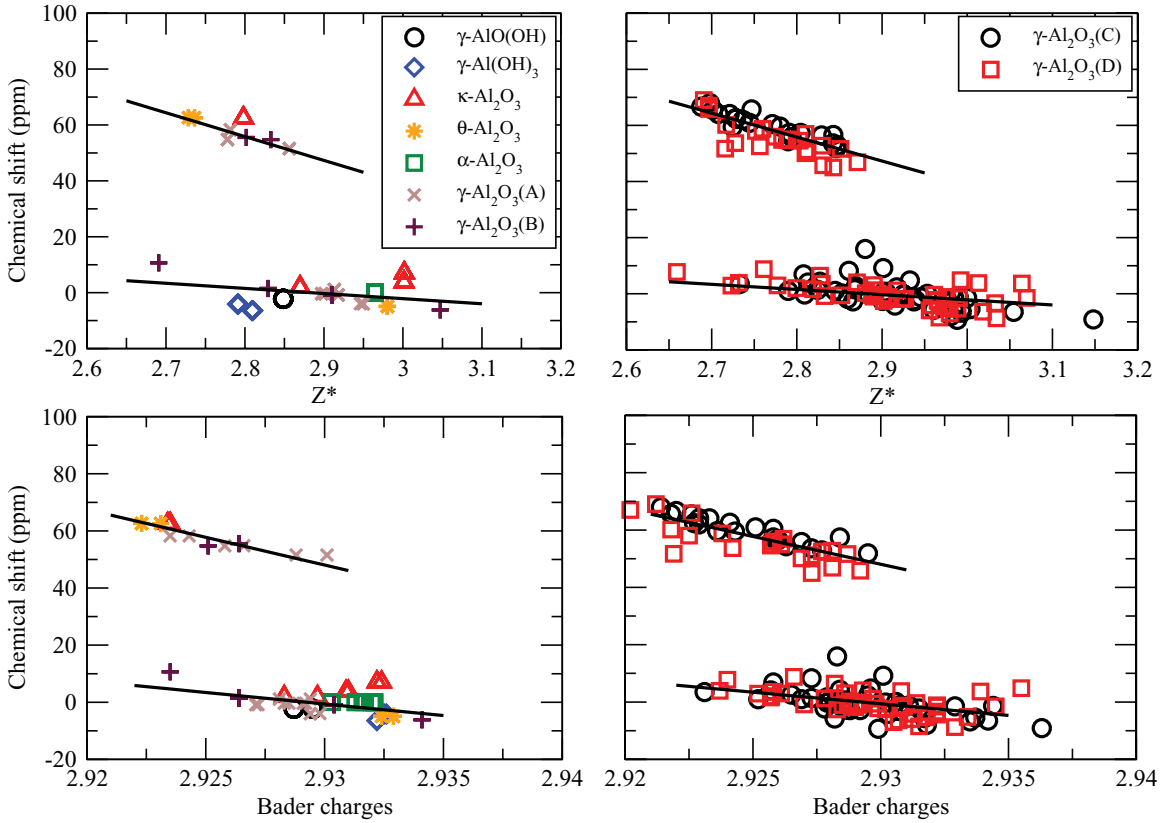

FIG. 6. (Color online) Correlations between chemical shifts and effective charges, Z^*, (above) or Bader charges (below). Left panels collect the data for all the structures considered in this work except the γ-alumina models C and D, which contain many different Al sites. For these models the data are reported separately in the right panels. Lines correspond to linear fit to Al_{oct} and Al_{tet} data for all the structures.

result in widely different distributions of NMR parameters for the same spectrum.

D. Correlation analysis

In the literature, there have been several attempts to correlate features in NMR spectra with local structural details such as coordination numbers,[22] local atomic bond length and angular distortion,[57] shortest bond length,[58] Mulliken charge population,[22] etc.

Our calculations confirm the dependence of chemical shifts on aluminium coordination numbers, such that four-, five- and six-coordinated aluminium sites show chemical shifts in well separated ranges: the lower the coordination number the larger is the chemical shift.

However, the internal distribution within a given coordination number does not correlate with local geometric descriptors such as local bond length, angular distortions,[57] or shortest bond length.[58] To explain this, we performed a simple test in the nonspinel model B for γ-alumina by displacing an oxygen atom, while keeping the rest fixed, and we observed that the NMR parameters were affected in a region extending up to the third coordination shell, thus demonstrating the sensitivity of NMR to nonlocal structural details.

The only properties that we found to display a significant correlation with the NMR shielding were aluminium Bader charges and Born dynamical effective charges. For both charges the correlation is linear and structure independent as demonstrated by the linear fits obeyed equally well by all phases, as shown in Fig. 6.

It should be mentioned that Bader charges and Born effective charges correlate very strongly with each other so that no additional information can be gained by considering the two charges together. This is because γ-alumina is a crystal with a high degree of ionicity, where these two quantities are strongly related.

Furthermore, we can understand the correlation of NMR shielding with Born effective charges because they both originate from local electronic susceptibility, one being determined from the current induced by the magnetic field, the other measuring the charge flow associated to vibrational motion.

As a historical curiosity, we mention that proposing a correlation between NMR chemical shifts and effective charges is not a complete novelty since in a couple of papers[59,60] in the late seventies a correlation was reported to exist for binary semiconductors among Szigeti's effective charges and ^{27}Al and ^{31}P NMR chemical shifts.

IV. CONCLUSIONS

We investigated from first principles the ^{27}Al NMR properties of several well characterized crystalline phases of Al_2O_3 and of two of its calcination precursor phases, obtaining very good agreement with available experimental results. New insight for the peak assignments in the spectra were proposed for some structures.

This gave confidence in the theoretical approach and allowed us to address the open problem of the structural characterization of the technologically important γ-alumina phase by comparing the experimental spectra with the theoretical predictions calculated for four structural models recently appeared in the literature: our study supports the model structure with $Fd\bar{3}m$ symmetry proposed by Paglia *et al.*[49] as the one that best reproduces the NMR experimental results in the bulk.

Calculations confirm that chemical shifts strongly depend on coordination number. Moreover, within a given coordination number, a linear correlation exists between chemical shifts and Born effective charges or Bader charges.

ACKNOWLEDGMENTS

We are grateful to Dr. L.A. O'Dell, Dr. M.E. Smith, and Dr. T. J. Bastow for providing their experimental NMR spectra and to Dr. Gonzalo Gutiérrez and Dr. Eduardo Menéndez-Proupin for providing their structural model. SdG and EK like to thank Davide Ceresoli for useful discussions and for suggesting the use of QUADFIT code for the simulation of spectra including quadrupolar interaction. ARF wishes to thank SISSA for the support and facilities during the obtention of the results. Calculations have been performed on the Sp6-IBM machine at CINECA in Bologna, Italy, and on the HPC cluster at SISSA. This work was also supported by Petrobras S.A. and Brazilian agencies CAPES, FAPEMIG, and CNPq.

[1] S. H. Cai, S. N. Rashkeev, S. T. Pantelides, and K. Sohlberg, Phys. Rev. B **67**, 224104 (2003).
[2] K. J. D. MacKenzie, J. Temuujin, and K. Okada, Thermochim. Acta **327**, 103 (1999).
[3] Y. Cesteros, P. Salagre, F. Medina, and J. E. Sueiras, Chem. Mater. **11**, 123 (1999).
[4] J. E. Brown, D. Clark, and W. W. Elliott, J. Chem. Soc. **13**, 84 (1953).
[5] D. B. Tilley and R. A. Eggleton, Clays Clay Min. **44**, 658 (1996).
[6] G. Ertl, H. Knözinger, and J. Weitkamp, *The Handbook of Heterogeneous Catalysis* (Wiley-VCH, Weinheim, 1997).
[7] M. Digne, P. Sautet, P. Raybaud, P. Euzen, and H. Toulhoat, J. Catal. **226**, 54 (2004).
[8] H. C. Stumpf, A. S. Russell, J. W. Newsome, and C. M. Tucker, Ind. Eng. Chem. **42**, 1398 (1950).
[9] R. Zhou and R. L. Snyder, Acta Crystallogr. Sect. B **47**, 617 (1991).
[10] M.-H. Lee, C.-F. Feng, V. Heine, and J. Klinowki, Chem. Phys. Lett. **265**, 673 (1997).
[11] J. A. Wang, X. Bokhimi, A. Morales, O. Novaro, T. López, and R. Gómez, J. Phys. Chem. B **B103**, 299 (1999).
[12] C. Wolverton and K. C. Hass, Phys. Rev. B **63**, 024102 (2000).
[13] K. Sohlberg, S. J. Pennycook, and S. T. Pantelides, Chem. Eng. Comm. **181**, 107 (2000).
[14] X. Krokidis, P. Raybaud, A. Gobichon, B. Rebours, P. Euzen, and H. Toulhoat, J. Phys. Chem. B **105**, 5121 (2001).
[15] P. Raybaud, M. Digne, R. Iftimie, W. Wellens, P. Euzen, and H. Toulhoat, J. Catal. **201**, 236 (2001).

[16]L. Smrcok, V. Langer, and J. Krestan, Acta Cryst. C**62**, i83 (2006).
[17]A. R. Ferreira, M. J. F. Martins, E. Konstantinova, R. B. Capaz, W. F. Souza, S. X. Chiaro, and A. A. Leitão, J. Solid State Chem. **184**, 1105 (2011).
[18]M. R. Hill, T. J. Timothy, J. Bastow, S. Celotto, and A. J. Hill, Chem. Mater. **19**, 2877 (2007).
[19]L. A. O'Dell, S. L. P. Savin, A. V. Chadwick, and M. E. Smith, Solid State Nucl. Magn. Reson. **31**, 169 (2007).
[20]C. J. Pickard and F. Mauri, Phys. Rev. B **63**, 245101 (2001).
[21]J. R. Yates, C. J. Pickard, and F. Mauri, Phys. Rev. B **76**, 024401 (2007).
[22]M. Choi, K. Matsunaga, F. Oba, and I. Tanaka, J. Phys. Chem. C **113**, 3869 (2009).
[23]R. Lizárraga, E. Holmström, S. C. Parker, and C. Arrouvel, Phys. Rev. B **83**, 094201 (2011).
[24]R. Bader, *Atoms in Molecules: A Quantum Theory* (Oxford University Press, New York, 1990); W. Tang, E. Sanville, and G. Henkelman, J. Phys. Condens. Matter **21**, 084204 (2009).
[25]M. Born and K. Huang, *Dynamical Theory of Crystal Lattices* (Oxford University Press, Oxford, 1954); H. Böttger, *Principles of the Theory of Lattice Dynamics* (Physik-Verlag, Weinheim, 1983).
[26]P. Giannozzi *et al.*, J. Phys. Condens. Matter **21**, 395502 (2009); See also http://www.quantum-espresso.org.
[27]P. Hohenberg and W. Kohn, Phys. Rev. **136**, B864 (1964).
[28]W. Kohn and L. J. Sham, Phys. Rev. **140**, A1133 (1965).
[29]J. P. Perdew, K. Burke, and M. Ernzerhof, Phys. Rev. Lett. **77**, 3865 (1996).
[30]Y. Zhang and W. Yang, Phys. Rev. Lett. **80**, 890 (1998).
[31]M. Dion, H. Rydberg, E. Schröder, D. C. Langreth, and B. I. Lundqvist, Phys. Rev. Lett. **92**, 246401 (2004).
[32]T. Thonhauser, V. R. Cooper, S. Li, A. Puzder, P. Hyldgaard, and D. C. Langreth, Phys. Rev. B **76**, 125112 (2007).
[33]P. E. Blöchl, Phys. Rev. B **50**, 17953 (1994).
[34]H. J. Monkhorst and J. D. Pack, Phys. Rev. B **13**, 5188 (1976).
[35]The *k*-point meshes for each structure are as follows: Boehmtie $3 \times 1 \times 3$, Gibbsite $2 \times 2 \times 2$, α-Al_2O_3 $2 \times 2 \times 1$, κ-Al_2O_3 $3 \times 2 \times 2$, θ-Al_2O_3 $1 \times 4 \times 2$, γ-Al_2O_3(A) $2 \times 2 \times 1$, γ-Al_2O_3(B) $2 \times 2 \times 1$, γ-Al_2O_3(C) $2 \times 2 \times 1$, and γ-Al_2O_3(D) $1 \times 2 \times 1$. All meshes were shifted by half of the mesh interval in each direction.
[36]P. Giannozzi, S. de Gironcoli, P. Pavone, and S. Baroni, Phys. Rev. B **43**, 7231 (1991).
[37]S. Baroni, S. de Gironcoli, A. Dal Corso, and P. Giannozzi, Rev. Mod. Phys. **73**, 515 (2001).
[38]T. F. Kempa and M. E. Smith, Solid State Nucl. Magn. Reson. **35**, 243 (2009).
[39]N. Ishizawa, T. Miyata, J. Minato, F. Marumo, and S. Iwai, Acta Crystallogr. Sect. B **36**, 228 (1980).
[40]B. Ollivier, R. Retoux, P. Lacorre, D. Massiot, and G. Férey, J. Mater. Chem. **7**, 1049 (1997).
[41]H. Saalfeld and M. Wedde, Z. Kristallogr. **139**, 129 (1974).
[42]A. Ramos-Gallardo and A. Vegas, Z. Kristallogr. **211**, 299 (1996); **296**, 572 (2006).
[43]A. N. Christensen, M. S. Lehmann, and P. Convert, Alta Chem. Scand **A36**, 303 (1982).
[44]K. Damodaran, P. R. Rajamohanan, and D. Chakrabarty, J. Am. Chem. Soc. **124**, 3200 (2002).
[45]G. Gutiérrez, A. Taga, and B. Johansson, Phys. Rev. B **65**, 012101 (2001).
[46]E. Menéndez-Proupin and G. Gutiérrez, Phys. Rev. B **72**, 035116 (2005).
[47]W. Y. Ching, L. Ouyang, P. Rulis, and H. Yao, Phys. Rev. B **78**, 014106 (2008).
[48]G. Paglia, Ph.D. thesis, Curtin University of Technology, 2004.
[49]G. Paglia, A. L. Rohl, C. E. Buckley, and J. D. Gale, Phys. Rev. B **71**, 224115 (2005).
[50]C. Loyola, E. Menéndez-Proupin, and G. Gutiérrez, J. Mater. Sci. **45**, 5094 (2009).
[51]A. Vyalikh, K. Zesewitz, and U. Scheler, Magn. Reson. Chem. **48**, 877 (2010).
[52]R. C. Slade, J. C. Southern, and I. M. Thompson, J. Mater. Chem. **1**, 563 (1991).
[53]S. E. Ashbrook, J. McManus, K. J. D. MacKenzie, and S. Wimperis, J. Phys. Chem. B **104**, 6408 (2000).
[54]J. H. Kwak, J. Z. Hu, D. H. Kim, J. Szanyi, and C. H. F. Peden, J. Catal. **251**, 189 (2007).
[55]C. Pecharromán, I. Sobrados, J. E. Iglesias, T. González-Carreño, and J. Sanz, J. Phys. Chem. B **103**, 6160 (1999).
[56]G. Paglia, C. E. Buckley, A. L. Rohl, B. A. Hunter, R. D. Hart, J. V. Hanna, and L. T. Byrne, Phys. Rev. B **68**, 144110 (2003).
[57]D. Mao, E. J. Walter, H. Krakauer, and Z. Wu, Phys. Rev. B **76**, 014105 (2007).
[58]D. L. Pechkis, E. J. Walter, and H. Krakauer, J. Chem. Phys. **135**, 114507 (2011).
[59]R. E. J. Sears, Phys. Rev. B **18**, 3054 (1978).
[60]R. E. J. Sears, Phys. Rev. B **22**, 1135 (1980).